JPET Fast Forward. Published on November 10, 2008 as DOI: 10.1124/jpet.108.146647

JPET#146647

Title Page

Physiologically Based Pharmacokinetic Modeling to Predict Transporter-Mediated Clearance and Distribution of Pravastatin in Humans

Takao Watanabe, Hiroyuki Kusuhara, Kazuya Maeda, Yoshihisa Shitara and Yuichi Sugiyama

Department of Molecular Pharmacokinetics, Graduate School of Pharmaceutical Sciences, The University of Tokyo, 7-3-1 Hongo, Bunkyo-ku, Tokyo 113-0033, Japan (T. W., H. K., K. M., Y. Su.)

Department of Biopharmaceutics, Graduate School of Pharmaceutical Sciences, Chiba University, 1-8-1 Inohana, Chuo-ku, Chiba 260-8657, Japan (Y. Sh.)

Running Title Page

Running title: PBPK Model to Predict Pharmacokinetics of Pravastatin

Corresponding Author: Yuichi Sugiyama, Ph. D.

Address: Department of Molecular Pharmacokinetics, Graduate School of Pharmaceutical Sciences, The University of Tokyo, 7-3-1 Hongo, Bunkyoku-Tokyo, 113-0033, Japan

Phone: +81-3-5841-4770

FAX: +81-3-5841-4766

e-mail: sugiyama@mol.f.u-tokyo.ac.jp

Number of text pages: 34

Number of tables: 3

Number of figures: 9

Number of references: 40

Number of words in the Abstract: 250

Number of words in the Introduction: 707

Number of words in the Discussion: 1331

Abbreviations:

PBPK, physiologically based pharmacokinetic; OATP, organic anion transporting polypeptide; MRP, multidrug resistance–associated protein; SF, scaling factor; CMV, canalicular membrane vesicle; statin, HMG-CoA reductase inhibitor; PAPS, 3′-phosphoadenosine 5′-phosphosulfate; i.v., intravenous; i.d., intraduodenal; AUC, area under the concentration–time curve; PS, permeability surface product; CL, clearance; $CL_{int,all}$, overall intrinsic clearance; inf, influx; dif, diffusion; met, metabolism; tot, total; B, blood

Abstract

Hepatobiliary excretion mediated by transporters, OATP1B1 and MRP2, is the major elimination pathway of an HMG-Co A reductase inhibitor, pravastatin. The present study examined the effects of changes in the transporter activities on the systemic and liver exposure of pravastatin using a physiologically based pharmacokinetic model. Scaling factors, determined by comparing *in vivo* and *in vitro* parameters of pravastatin in rats for the hepatic uptake and canalicular efflux, were obtained. The simulated plasma and liver concentrations, and biliary excretion profiles were very close to the observed data in rats under linear and nonlinear conditions. *In vitro* parameters, determined in human cryopreserved hepatocytes and canalicular membrane vesicles, were extrapolated to *in vivo* parameters using the scaling factors obtained in rats. The simulated plasma concentrations of pravastatin were close to the reported values in humans. Sensitivity analyses showed that changes in the hepatic uptake ability altered the plasma concentration of pravastatin markedly, but had a minimal effect on the liver concentration, while changes in the ability of canalicular efflux altered the liver concentration of pravastatin markedly, but had a small effect on the plasma concentration. In conclusion, the model allows the prediction of the disposition of pravastatin in humans. The present study suggests that changes in the OATP1B1 activities may have a small and a large impact on the therapeutic efficacy and side effect (myopathy) of pravastatin, respectively, whereas those in the MRP2 activities may have opposite impacts (i.e., a large and a small impact on the therapeutic efficacy and side effect).

Introduction

Predicting the disposition of drugs in humans, particularly in the early stages of drug development, has been a critical issue in selecting the proper candidate drugs, because the exposure of drugs to target organs is the major factor determining their pharmacological and/or toxicological activity. Human liver microsomes allow the reliable prediction of the metabolic clearance of drugs in humans (Rane et al., 1977; Iwatsubo et al., 1997; Obach, 1999; Naritomi et al., 2001). Biliary excretion, another hepatic elimination pathway, is the major systemic elimination pathway, particularly for amphipathic anionic drugs such as HMG-CoA reductase inhibitors (statins) and angiotensin II receptor antagonists. Since multiple transporters on the sinusoidal and canalicular membranes are involved, it is necessary to separately determine three kinetic parameters (1) uptake, (2) sinusoidal efflux, and (3) canalicular efflux, to predict biliary clearance with regard to the plasma concentration (Giacomini and Sugiyama, 2005; Shitara et al., 2006a). The uptake clearance determined in freshly isolated rat hepatocytes correlates well with that determined with the multiple indicator dilution method (Miyauchi et al., 1993), and rat hepatocytes are reported to be a useful tool for predicting the hepatic clearance of drugs with significant hepatic uptake (Soars et al., 2007). Although cryopreserved human hepatocytes and canalicular membrane vesicles (CMVs) are commercially available, their usefulness in predicting *in vivo* hepatic uptake and canalicular efflux clearance remains to be examined. No method to quantify *in vitro* sinusoidal efflux has yet been established.

A physiologically based pharmacokinetic (PBPK) model, in which compartments representing tissues are connected with the blood flow, has been used to predict the time profiles of plasma and tissue concentrations (Kawai et al., 1998; Jones et al., 2006). The PBPK model is quite useful for simulating the effects of drug–drug interactions and genetic variations in drug-metabolizing enzymes and transporters on the exposure of drugs to the blood and organs, and ultimately their effects on the pharmacological actions of drugs (Jones et al., 2006; Shitara and Sugiyama, 2006a). The purpose of this study was to establish a PBPK model to describe the

disposition of pravastatin for which transporters are deeply involved in its hepatobiliary transport. Pravastatin, one of the statins used for the treatment of hyperlipidemia, was selected as the model compound in this study. The liver is a target organ for the pharmacological actions of statins, whereas myotoxic adverse effects, sometimes severe, including myopathy or rhabdomyolysis, are associated with the use of statins. Therefore, it is very important to simulate the exposure of statins to the liver and skeletal muscle to predict their pharmacological and toxicological effects. Hepatobiliary transport is the main elimination pathway of pravastatin from the systemic circulation and is mediated by uptake and efflux transporters in the liver (Shitara and Sugiyama, 2006b). The hepatic uptake of pravastatin is mainly mediated by organic anion transporting polypeptide 1B1 (OATP1B1), and its biliary excretion is predominantly mediated by multidrug resistance–associated protein 2 (MRP2) (Yamazaki et al., 1993; Yamazaki et al., 1997; Nakai et al., 2001). Pravastatin undergoes urinary excretion by tubular secretion as well as by glomerular filtration in humans (Singhvi et al., 1990). Organic anion transporter 3 (OAT3) has been suggested to be responsible for the basolateral uptake of pravastatin in rats and humans (Hasegawa et al., 2002; Nakagomi-Hagihara et al., 2007), whereas the transporter involved in its luminal efflux is yet to be identified.

In this study, *in vivo* experiments were carried out using male rats to obtain concentration–time profiles of pravastatin in the plasma, liver, kidney, muscle, brain, and lung. The kinetic parameters for the hepatic uptake and canalicular efflux of pravastatin were determined from *in vitro* transport studies using freshly isolated rat hepatocytes and CMVs, respecitvely. *In vitro–in vivo* scaling factors (SFs) were obtained for the hepatic uptake and subsequent canalicular efflux of pravastatin in rats. A PBPK model was constructed to simulate the systemic and liver exposure of pravastatin in rats. Using the PBPK model, the SFs determined in rats and kinetic parameters determined using human materials, the plasma concentration-time curve of pravastatin in humans was also simulated. Finally, the effects of changes in these transporter activities, caused by genetic polymorphisms and drug-drug

interactions, on the concentration profiles of pravastatin in plasma and the liver were examined using the PBPK model.

Methods

Materials

[^{3}H]Pravastatin (45.5 Ci/mmol), unlabeled pravastatin, and a pravastatin analogue, R-122798 ((3*R*,5*R*)-3,5-dihydroxy-7-[(1*S*,2*S*,6*S*,8*S*,8a*R*)-6-hydroxy-8-(isobutyryloxy)-2-methyl-1,2,6,7,8,8a-hexahydronaphthalen-1-yl]heptanoic acid), were provided by Daiichi Sankyo Co., Ltd (Tokyo, Japan). Cryopreserved human hepatocytes and human liver S9 fractions were purchased from In Vitro Technologies (Baltimore, MD). Human liver S9 fractions were also purchased from Xenotech LLC (Lenexa, KS) and Tissue Transformation Technologies (Edison, NJ). All other chemicals and reagents were of analytical grade and were readily available from commercial sources.

Animals

Male Sprague Dawley rats (6–7 weeks old) were purchased from Nippon SLC (Shizuoka, Japan). All animals were maintained under standard conditions with a reversed light/dark cycle and were treated humanely. Food and water were available ad libitum. The studies were carried out in accordance with the guidelines of the Institutional Animal Care Committee, Graduate School of Pharmaceutical Sciences, The University of Tokyo, Tokyo, Japan.

Animal Experiments

Male Sprague Dawley rats, weighing approximately 250–320 g, were used throughout the experiments. Under ether anesthesia, the femoral artery was cannulated with a polyethylene catheter (SP-31) for the collection of blood samples. The bile duct was cannulated with a polyethylene catheter (PE-10) for bile collection, and the bladder was cannulated with a silicon catheter to collect urine. The femoral vein or the duodenum was cannulated with a polyethylene catheter (SP-31) for the administration of pravastatin. Each rat was placed in a Bollman cage and allowed to recover from the anesthesia before the experiments were continued. The rats

were given pravastatin intravenously (i.v.) at 0.2, 1, 10, 50, or 200 mg/kg or intraduodenally (i.d.) at 20 mg/kg. Blood samples were collected at the designated times and centrifuged at 1500 × *g* for 10 min at 4 °C to obtain plasma. Bile and urine samples were collected in preweighed test tubes at the designated intervals throughout the experiment. After the last blood sample had been taken, each rat was killed and the liver, kidney, brain, lungs, and skeletal muscle were excised immediately for the tissue distribution study. The tissues were weighed and flash frozen in liquid nitrogen. All the samples were stored at –20 °C until quantification.

Transport Study Using Human Cryopreserved Hepatocytes

This experiment was performed as described previously (Shitara et al., 2003). Briefly, immediately before the study, the hepatocytes were thawed at 37 °C. After they had been washed twice with ice-cold Krebs–Henseleit buffer, the cells were resuspended in Krebs–Henseleit buffer to a cell density of 1.0×10^6 viable cells/mL for the uptake study. After preincubation of the cells (1.2×10^5 cells/reaction) at 37 °C for 3 min, drug uptake was initiated by the addition of labeled and unlabeled substrates to the cell suspension. The reaction was terminated after 0.5 or 2 min by separating the cells from the substrate solution. For this purpose, an aliquot of 100 μL of incubation mixture was placed in a centrifuge tube (450 μL) containing 50 μl of 2 N NaOH under a layer of 100 μL of oil (density = 1.015, a mixture of silicone oil and mineral oil; Sigma-Aldrich, St Louis, MO). The sample tube was centrifuged for 10 s in a tabletop centrifuge (10,000 × *g*; Beckman Microfuge E; Beckman Coulter, Fullerton, CA). After overnight incubation in alkali to dissolve the hepatocytes, the centrifuge tube was cut and each phase was transferred to a scintillation vial. The phase containing the dissolved cells was neutralized with 50 μL of 2 N HCl, mixed with scintillation cocktail, and its radioactivity was measured in a liquid scintillation counter (LS6000SE; Beckman Coulter). The time course for the uptake of [^{3}H]pravastatin into hepatocytes was expressed as the uptake volume (μL/10^6 viable cells) of the radioactivity taken up into the cells (dpm/10^6 cells) divided

by the concentration of radioactivity in the incubation buffer (dpm/μL). The initial uptake velocity of [^{3}H]pravastatin was calculated from the slopes of the uptake volume versus time plots obtained at 0.5 and 2 min, and expressed as the uptake clearance (μL/min per 10^6 cells).

Metabolism Study Using the Liver S9 Fraction

It has been reported that pravastatin is metabolized by sulfotransferase in male rats (Kitazawa et al., 1993). Therefore, we used the liver S9 fraction as the enzyme source. The liver S9 fraction was prepared from four rats using standard procedures and stored at –80 °C until use. The protein concentration was determined by the Lowry method, using bovine serum albumin as the standard. Pravastatin was incubated with a reaction mixture consisting of rat liver S9 fraction (final concentration, 8 mg/mL), NADPH-generating system (0.8 mM $NADP^+$, 8 mM glucose-6-phosphate, 1 U/mL glucose-6-phosphate dehydrogenase, and 3 mM $MgCl_2$), and 3′-phosphoadenosine 5′-phosphosulfate (PAPS; final concentrations, 0.5 and 5 mM for low and high pravastatin concentrations, respectively) in the presence of 100 mM phosphate buffer (pH 7.4). After preincubation at 37 °C for 10 min, pravastatin (final concentration, 0.1–500 μM) was added to initiate the enzyme reaction. At the designated time, the reactions were terminated by mixing them with equal volumes of methanol containing R-122798, an analytical internal standard, followed by centrifugation at 15,000 × *g* for 10 min at 4 °C. The supernatant was subjected to liquid chromatography/mass spectrometry (LC/MS) analysis. In studies with the human liver S9 fraction, the concentrations of pravastatin and PAPS were 5 μM and 1 mM, respectively; other incubation conditions were the same as in the rat studies.

LC/MS Analysis

Liver, kidney, brain, lung, and skeletal muscle were added to 3–5 volumes of physiological saline (w/v) and homogenized. Tissue homogenates, plasma, bile, and urine samples were deproteinated with two volumes of methanol containing the internal standard (1

μg/mL R-122798) and centrifuged at 15,000 × *g* for 10 min at 4 °C. High-concentration samples were diluted appropriately with blank matrix before deproteination. The supernatant was subjected to LC/MS analysis. The appropriate standard curves were prepared in the equivalent blank matrix and used for each analysis.

The LC/MS consisted of an Alliance HT 2695 separation module with an autosampler (Waters, Milford, MA) and a Micromass ZQ mass spectrometer with an electron ion spray interface (Waters). The optimum operating conditions used were: electrospray probe (capillary) voltage, 3.2 kV; sample cone voltage, 20 V; and source temperature, 100 °C. The spectrometer was operated at a drying desolvation gas flow rate of 350 L/h. The mass spectrometer was operated in the selected ion monitoring mode using the respective MH^- ions *m/z* 423.3 for pravastatin and *m/z* 409.3 for the internal standard. The mobile phase used for high-performance liquid chromatography was acetonitrile/ammonium acetate buffer (10 mM, pH 4) = 7/3 (v/v) and the flow rate was 0.3 mL/min. Chromatographic separation was achieved on a C18 column (Inertsil ODS-3 column, 50 × 2.1 mm; particle size, 3 μm) (GL Sciences, Tokyo, Japan).

Data Analysis of Metabolic Clearance in Liver S9

The metabolic velocity was calculated from the slope of the natural log (concentration)–time plot. Because the Eadie–Hofstee plot showed curvature, the kinetic parameters were obtained using the following equation:

$$v = \frac{V_{\max 1} \times S}{K_{m1} + S} + \frac{V_{\max 2} \times S}{K_{m2} + S} \quad \text{Eq.1}$$

where v is the initial velocity (pmoles/min per mg protein), S is the substrate concentration (μM), $V_{\max 1}$ and $V_{\max 2}$ are the maximum velocities (pmoles/min per mg protein), and K_{m1} and K_{m2} are the Michaelis constants (μM). Fitting was performed with the nonlinear least-squares method

using the MULTI program (Yamaoka et al., 1981). The input data were weighted as the reciprocals of the observed values and the Damping Gauss–Newton algorithm was used for fitting.

Model Development

The PBPK model was constructed to describe the pharmacokinetics of pravastatin in rats and humans (Fig. 1). The key features of this model are as follows. (1) Active uptake (PS_{inf}) and passive diffusion clearances (PS_{dif}) on the sinusoidal membrane, and biliary clearance (PS_{bile}) on the canalicular membrane in the liver are incorporated. (2) The liver compartment consists of five units of extracellular and subcellular compartments, connected by blood flow in tandem, to fit the hepatic disposition to the "dispersion" model. Because the hepatic elimination of pravastatin in rats is blood-flow limited, the "dispersion" model is the appropriate model for the hepatic elimination of such high-clearance drugs (Roberts and Rowland, 1986; Iwatsubo et al., 1997; Naritomi et al., 2001). The number of liver compartments was determined by comparing the hepatic availability ($F_{h,n}$) and F_h predicted using the dispersion model. $F_{h,n}$ is the product of the availability in the liver compartments (Eq.2).

$$F_{h,n}=(Q/(Q+f_B(CL_{int,all}/n)))^n \quad \text{Eq.2}$$

where "n" represents the number of compartments. The integer number "n" which gave the $F_{h,n}$ value closest to that in the dispersion model was selected. (3) The brain and muscle, target tissues for the adverse effects of statins, were included. (4) Although urinary excretion is a minor elimination pathway in male rats, the kidney was included because the kidney-to-blood concentration ratio for pravastatin is high in male rats, probably because of the efficient uptake and/or reabsorption of pravastatin. Indeed, the renal clearance of pravastatin in male rats was lower than the glomerular filtration rate corrected by the blood unbound fraction. In contrast, renal clearance must be taken into consideration in humans. Because this study focused on

hepatobiliary transport, renal elimination occurs from the systemic compartment. (5) The rapid equilibrium distribution of pravastatin between the blood and tissues other than the liver was assumed. (6) The initial distribution volume, estimated by fitting the plasma concentration time profiles of pravastatin in rats after the intravenous administration of 0.2 and 1 mg/kg to a two-compartment model, was used as the volume of the rapid equilibrium compartment including the blood compartment, and it was assumed that there is no interspecies difference in the initial distribution volume. The differential equations are shown in Appendix I, and all simulations were performed with SAAM II (SAAM Institute, Seattle, WA).

Estimation of Kinetic Parameters Used in the Simulation

In vitro parameters (rats and humans)

The *in vitro* active uptake ($PS_{inf,vitro}$) and passive diffusion clearances ($PS_{dif,vitro}$) of pravastatin on the sinusoidal membrane were determined from the uptake studies using isolated hepatocytes. The parameters for rats were taken from previous reports (Yamazaki et al., 1993; Ishigami et al., 1995) and those for humans were determined in the present study. $PS_{inf,vitro}$ and $PS_{dif,vitro}$ were regarded as the saturable and nonsaturable components, respectively, in the uptake clearance into hepatocytes. A physiological scaling factor of 1.2×10^8 cells/g liver was used for scaling-up to the organ level (Iwatsubo et al., 1997). The *in vitro* biliary clearance ($PS_{bile,vitro}$) of pravastatin was calculated from the ATP-dependent uptake clearance into the CMVs using the following equation (Niinuma et al., 1999)

$$PS_{bile,vitro} = (V_{initial} \times R) / (E \times IO) \quad \text{Eq.3}$$

where $V_{initial}$ represents the velocity of the initial ATP-dependent uptake by CMVs corrected by medium concentration (6.08 μL/min per mg protein for rats and 1.90 μL/min per mg protein for humans), R represents the recovery of liver homogenate protein (174 mg homogenate protein/g liver for rats and 133 mg homogenate protein/g liver for humans), E represents the enrichment of the CMV fraction (70.4 for rats and 61.8 for humans), and IO represents the population of

inside-out CMVs (0.347 for rats and 0.555 for humans).

In vivo parameters (rats)

The *in vivo* intrinsic biliary clearance ($PS_{bile,vivo}$) at the canalicular membrane was calculated by dividing the biliary excretion rate by the hepatic unbound concentration at steady state (Yamazaki et al., 1996b; Yamazaki et al., 1997). Systemic elimination other than biliary excretion was regarded as the hepatic metabolism because renal elimination in male rats is negligible. *In vivo* intrinsic metabolic clearance ($CL_{met,int,vivo}$) was thus obtained with the following equation:

$$CL_{met,\,int,\,vivo} = PS_{bile,\,vivo} \times \frac{100 - (\%\ \text{of excretion into bile at 0.2mg/kg})}{(\%\ \text{of excretion into bile at 0.2mg/kg})} \quad \text{Eq.4}$$

The *in vivo* passive diffusion clearance on the sinusoidal membrane was assumed to be the same as $PS_{dif,vitro}$. The *in vivo* active uptake clearance ($PS_{inf,vivo}$) was estimated from:

$$PS_{inf,vivo} = CL_{int,all} \times \frac{PS_{dif,vivo} + PS_{bile,vivo} + CL_{met,int,vivo}}{PS_{bile,vivo} + CL_{met,int,vivo}} - PS_{dif,vivo} \quad \text{Eq.5}$$

where $CL_{int,all}$ represents the overall hepatic intrinsic clearance estimated from the hepatic availability using the "dispersion" model, with a dispersion number of 0.17, which was obtained by dividing the bioavailability by the fraction absorbed (Komai et al., 1992), assuming negligible metabolism in the small intestine. The average of the tissue-to-blood concentration ratios at 30, 60 and 90 min after the i.v. administration at 10mg/kg pravastatin were used as the tissue-to-blood partition coefficient (Kp), assuming a pseudo-steady-state (Table 2). Actually, the tissue-to-blood concentration ratios at 30, 60 and 90 min were similar (muscle, 0.28, 0.21 and 0.18; brain, 0.045, 0.029 and 0.034; kidney, 13, 14 and 15; lung, 0.76, 0.67 and 0.77 at 30, 60 and 90 min, respectively). The absorption rate constants were estimated by noncompartment analysis using the plasma concentration data.

Results

In vivo Pharmacokinetics of Pravastatin in Rats

Figure 2 shows time profiles of the plasma concentration of pravastatin following its i.v. (0.2 mg/kg) and i.d. (20 mg/kg) administration, and the cumulative amount of pravastatin excreted into the bile. The total blood clearance ($CL_{tot,B}$) was similar to the hepatic blood flow rate. The bioavailability of pravastatin after i.d. administration was calculated to be 0.0087 by comparing the AUCs for pravastatin after i.v. and i.d. administration. Forty-six percent of the dose was recovered in the bile as the parent compound following i.v. administration, whereas the amount excreted into the urine was less than 4% of the dose. Even after i.d. administration, 33% was recovered in the bile.

The nonlinearity of the disposition of pravastatin was examined. The plasma concentrations and cumulative amounts excreted into the bile after its i.v. administration were determined at doses ranging from 0.2 to 200 mg/kg (Fig. 3). $CL_{tot,B}$ was independent of the dose up to 50 mg/kg, but decreased to 27 mL/min per kg at 200 mg/kg pravastatin. The cumulative biliary excretion increased slightly from 46% to 60% at doses above 0.2 mg/kg and was significantly delayed at 200 mg/kg.

Hepatic Metabolism of Pravastatin in Rats

The metabolism of pravastatin in the liver was examined using S9 fractions prepared from rat liver. It exhibited biphasic kinetics with high-affinity (K_{m1} 0.846 ± 0.403 μM; V_{max1} 4.47 ± 1.92 pmol/mg per min) and low-affinity (K_{m2} 80.3 ± 12.6 μM; V_{max2} 240 ± 16.2 pmol/mg per min) components (mean ± SD). The sum of the *in vitro* metabolic clearance for the high- and low-affinity components, corrected with the physiological scaling factor of 96.1 mg protein/g liver, was used as the *in vitro* metabolic clearance ($CL_{met,int,vitro}$), which was 0.793 ml/min per g liver (Table 1).

Simulation of Concentration–Time Profiles of Pravastatin in Rats

All parameters used in the simulation are summarized in Tables 1 and 2. The initial distribution volume was estimated to be 0.393 L/kg from the plasma concentration profile after the i.v. administration of 0.2 mg/kg pravastatin, which was used as the volume of the rapid equilibrium compartment in the model. Figures 2 and 3 show the simulated plasma concentrations and biliary excretion time profiles for pravastatin, together with the observed data after its i.v. and i.d. administration. To reproduce the *in vivo* pharmacokinetic profiles using *in vitro* parameters, SFs were necessary. For the *in vitro–in vivo* extrapolation of the transporter-mediated clearances, the ratio of the *in vivo* to the *in vitro* intrinsic clearances of each process in rats was given as the SF (Table 1). Furthermore, using the K_m values, the simulated plasma concentration and biliary excretion time profiles gave similar values to the observed data, even under nonlinear conditions. This model reproduced the time profiles for pravastatin in the liver and other peripheral tissues after its i.v. administration (Figs 4 and 5). In particular, the nonlinearity of the liver concentration–time profiles could also be simulated (Fig. 4). Although the model reasonably describes the experimental data, the simulated lines showed some deviation from the observed data at the terminal phase in Fig. 2 (left panel) and Fig. 5. This may be caused by the lack of a compartment corresponding to the organ which is associated with the terminal phase of systemic pravastatin. Moreover, the simulation results of biliary excretion of pravastatin administered at 1mg/kg and 10mg/kg showed some deviation from the observed data (Fig. 3, right panel). Since hepatic metabolism is saturated at these doses, this may be attributed to the deviation of the K_m value for metabolism.

Prediction of Pharmacokinetics in Humans

The uptake clearance determined using eight lots of human cryopreserved hepatocytes was 4.5 ± 2.9 μL/min per 10^6 cells at 1 μM pravastatin and 0.77 ± 0.63 μL/min per 10^6 cells at 100 μM pravastatin (mean ± SD). Using the physiological scaling factor of 1.2×10^8 cells/g

liver, $PS_{inf,vitro,human}$ and $PS_{dif,vitro,human}$ were calculated to be 0.448 mL/min per g liver and 0.0924 mL/min per g liver, respectively (Table 1). Unlike the rat liver S9 fraction, no metabolism of pravastatin was observed up to 180 min in the human liver S9 fractions purchased from three different vendors. Thus, the hepatic metabolism of pravastatin might be negligible in the human liver. The *in vivo* kinetic parameters for pravastatin in humans were predicted by multiplying the corresponding *in vitro* parameters obtained using human materials by the SF obtained from rat studies. For PS_{bile}, the saturable (ATP-dependent) biliary clearance in humans was predicted as described above and the nonsaturable component of the biliary clearance in humans was assumed to be the same as that in rats. Thus, the predicted $PS_{bile, vivo, human}$ was 0.388 mL/min per g liver. Assuming that the distribution of pravastatin to the tissues, except the liver, occurs by passive diffusion, the tissue-to-blood partition coefficient (Kp) was calculated by the following equation.

$$Kp=f_B/f_T$$

where f_B and f_T represent the blood unbound fraction (= plasma unbound fraction / blood-to-plasma concentration ratio) and the unbound fraction in the tissues, respectively. It was assumed that there is no species difference in f_T between rats and humans based on the previous report by Sawada et al. (1985). The estimated or reported physiological, anatomical, and kinetic parameters for humans used in the simulation are shown in Tables 1 and 2. Using these parameters, the plasma concentration–time profiles for pravastatin in humans after i.v. or oral administration were predicted. A lag time of 17 min was taken into consideration in the simulation of oral administration. The predicted concentration–time profiles were similar to the observed data (Fig. 6).

Effect of Transporter Activity on Systemic and Target Exposure

Sensitivity analyses were performed to understand the effects of the changes in transporter activities on the time profiles for the plasma and liver (a target organ) concentrations

of pravastatin in humans. The plasma and liver concentrations after the oral administration (40 mg) of pravastatin were simulated using the PBPK model constructed in this study, with varying hepatic transport activities over a range of 0.33–3.0 times the initial value. The simulated concentration–time profiles and the changes in the AUCs are shown in Fig. 7 and Table 3, respectively. Changes in the active hepatic uptake ability affected the plasma concentration profiles dramatically, but did not greatly affect the liver concentration profiles. On the contrary, changes in the ability of canalicular efflux altered the liver concentration of pravastatin markedly, but had a small effect on the plasma concentration. Changes in the passive diffusion clearance hardly affect the plasma and the liver concentration profiles.

Discussion

It is now well recognized that drug transporters play important roles in the processes of absorption, distribution, and excretion (Giacomini and Sugiyama, 2005; Shitara et al., 2006a). The purpose of this study was to construct a PBPK model to evaluate the concentration–time profiles for drugs in the plasma and peripheral organs in humans using physiological parameters, SFs, drug-related parameters (unbound fraction, and metabolic and membrane transport clearances extrapolated from *in vitro* experiments). The principle of the prediction was as follows. First, SFs were obtained by comparing *in vitro* and *in vivo* parameters in rats. Then, the *in vitro* human parameters were extrapolated *in vivo* using the SFs obtained in rats (Naritomi et al., 2001). Pravastatin was selected as the model compound because many studies have investigated the mechanisms involved in the drug disposition in rodents, and clinical data following intravenous and oral administration are available.

Consistent with a previous report (Yamazaki et al., 1996a), the hepatic elimination of pravastatin is blood-flow limited. Considering that the maximum amount of intact pravastatin excreted into the bile was 50%, it is likely that pravastatin undergoes hepatic metabolism in rats because pravastatin is excreted negligibly in the urine. Indeed, incubating pravastatin with the rat liver S9 fractions caused a reduction in intact pravastatin with time, and consisted of two different mechanisms with high- and low-affinity sites. The kinetic parameters related to hepatic clearance (PS_{inf}, PS_{dif}, PS_{bile}, and $CL_{met,int}$) were estimated from various *in vivo* experiments, and were incorporated into the PBPK model. As a result, plasma concentration and biliary excretion–time profiles for pravastatin were successfully reproduced (Figs 2–5). Moreover, nonlinear pharmacokinetics were also reproduced using the K_m values for hepatic uptake, biliary excretion, and metabolic clearances (Fig. 3). The liver concentrations of pravastatin were similar to the observed data, even under nonlinear conditions (200 mg/kg) (Fig. 4). These results suggest that the PBPK model constructed in this study is appropriate for describing the pharmacokinetics of pravastatin in rats.

The kinetic parameters PS_{inf}, PS_{dif}, and PS_{bile} were also determined *in vitro* using rat hepatocytes and CMVs, to obtain the relevant SFs (Table 2). The corresponding parameters were also determined using human cryopreserved hepatocytes and CMVs. These parameters were extrapolated *in vivo* using the SFs determined in rats. Because there is no evidence that active transport mechanisms are involved in the sinusoidal efflux of pravastatin, the clearance corresponding to the nonsaturable component (PS_{dif}) of the uptake was used as the clearance for sinusoidal efflux. Unlike the rat liver S9 fractions, pravastatin was not metabolized in the human liver S9 fractions. Therefore, the metabolic clearance was set to zero in humans. Using the human parameters, simulated plasma concentration–time profiles of pravastatin after the intravenous and oral administration were fairly close to the observed data for humans (Fig. 6), showing that the predicted value was not far from the true value. It should be noted that the sinusoidal efflux clearance (passive diffusion clearance) was lower than the intrinsic biliary clearance with regard to the liver concentration, indicating that the hepatobiliary transport of pravastatin is likely uptake-limited, and that the hepatic intrinsic clearance can be approximated to PS_{inf} (Shitara et al., 2006a). Therefore, even though the predictability of the absolute values for biliary and sinusoidal efflux clearance is low, the simulated results will be close to the observed data as far as the uptake clearance is correctly predicted. To validate the predictability of those clearances, the liver concentrations must be determined in humans, which should be possible with imaging technologies such as positron emission tomography, single-photon emission computed tomography, and magnetic resonance imaging. Recently, Ghibellini et al. (2007) have developed a methodology for the real-time measurement of the biliary excretion profiles of drugs in humans using a gamma scintigraphy technique. Further efforts are required to use such *in vivo* imaging technologies to increase the predictability of these pharmacokinetic parameters.

To date, clinical studies have demonstrated that the genetic variations of OATP1B1 and drug-drug interactions involving OATP1B1 are associated with interindividual differences in the

systemic exposure of pravastatin and other substrate drugs (Nishizato et al., 2003; Maeda et al., 2006; Niemi et al., 2006; Shitara and Sugiyama, 2006b). Because the pharmacological target of pravastatin is inside the cell, the liver exposure is a critical factor for its pharmacological activities. Based on the pharmacokinetic concepts, the AUC in the liver concentration is governed only by the sequestration clearance from the liver as far as the renal elimination is negligible, and is independent of the change in uptake clearance (see Appendix II). When renal clearance makes a significant contribution, the changes in hepatic uptake activity can affect both the liver and the plasma AUCs (Fig. 9, Appendix II). Actually, the renal elimination of pravastatin makes a significant contribution to the total body clearance (47% of the total body clearance) (Singhvi et al., 1990). Therefore, it is possible that the liver concentrations of pravastatin are affected to some extent also by the changes in the hepatic uptake activity. To support this concept, a simulation was performed with different uptake clearances (Fig. 7). Changes in the hepatic uptake clearance had a great impact on the plasma concentrations of pravastatin, but less impact on the liver concentrations. Accordingly, the effects of the genetic polymorphisms of OATP1B1 on the cholesterol-lowering effects of pravastatin will be small, or absent at least at steady-state (in other words after relatively long-term treatment). Indeed, the alteration of pharmacological effect of pravastatin with its chronic administration has not been observed in subjects with OATP1B1 polymorphisms although alteration of inhibitory effect of HMG CoA reductase activities in short-term treatments was reported (Takane et al., 2006; Kivisto and Niemi, 2007; Zhang et al., 2007). In contrast, changes in the intrinsic canalicular efflux activity should dramatically affect the liver concentration of pravastatin, while the plasma concentration is not affected as much by changes in the intrinsic biliary clearance (Fig. 7). Because the biliary excretion of pravastatin is mainly mediated by MRP2, the factors affecting MRP2 function, such as the use of MRP2 inhibitors or the genetic mutations causing Dubin–Johnson syndrome, will affect the pharmacological action of pravastatin. Furthermore, changes in the sinusoidal efflux clearance had only a slight impact on both the plasma and the liver

concentrations. This is because, even under these conditions, the uptake process is still the rate-limiting process. Although the predictability of the sinusoidal efflux clearance remains unknown, changes within this range will not affect the simulated results.

One of the serious adverse effects of statins is myopathy (rhabdomyolysis). Since its target organ is the skeletal muscle, the systemic exposure should be the determinant factor of this adverse effect. The sensitivity analyses showed that the changes in the hepatic uptake clearance had a great impact on the systemic exposure of pravastatin, while those in the canalicular efflux had a minimal impact (Fig.7). The results suggest that patients with an impaired OATP1B1 might be more susceptible to pravastatin-induced myopathy than those with normal one. Indeed, Morimoto et al. (2004) reported that the frequency of the OATP1B1 *15 haplotype was significantly higher in patients who experienced myopathy after receiving pravastatin or atorvastatin (which is also an OATP1B1 substrate) than in patients without myopathy, and a genomewide study elucidated that the variants in OATP1B1 are strongly associated with an increased risk of simvastatin-induced myopathy (Link et al., 2008).

In the present study, a PBPK model, including transporter-mediated membrane transport processes, was constructed, which allows the prediction of the pharmacokinetics of pravastatin in humans. It also extends our understanding of the effects of changes in the transport processes on the pharmacological and adverse effects of drugs by simulating the exposure of the systemic circulation and tissues to them. The present study suggests that changes in the OATP1B1 activities may have a small and a large impact on the therapeutic efficacy and side effect (myopathy) of pravastatin, respectively, whereas those in the MRP2 activities may have opposite impacts (i.e., a large and a small impact on the therapeutic efficacy and side effect).

Acknowledgments

We thank Ayako Takada and Yuji Sekiya for their excellent technical assistance.

References

Davies B and Morris T (1993) Physiological parameters in laboratory animals and humans. *Pharm Res.* **10**:1093-1095.

Ghibellini G, Vasist LS, Leslie EM, Heizer WD, Kowalsky RJ, Calvo BF and Brouwer KL (2007) In vitro-in vivo correlation of hepatobiliary drug clearance in humans. *Clin Pharmacol Ther.* **81**:406-413.

Giacomini KM and Sugiyama Y (2005) Membrane transporters and drug response, in Goodman & Gilman's The Pharmacological Basis of Therapeutics 11th edition (Brunton LL, Lazo JS, and Parker KL eds) pp 41-70, McGraw-Hill, New York.

Hasegawa M, Kusuhara H, Sugiyama D, Ito K, Ueda S, Endou H and Sugiyama Y (2002) Functional involvement of rat organic anion transporter 3 (rOat3; Slc22a8) in the renal uptake of organic anions. *J Pharmacol Exp Ther.* **300**:746-753.

Ishigami M, Tokui T, Komai T, Tsukahara K, Yamazaki M and Sugiyama Y (1995) Evaluation of the uptake of pravastatin by perfused rat liver and primary cultured rat hepatocytes. *Pharm Res* **12**:1741-1745.

Iwatsubo T, Hirota N, Ooie T, Suzuki H, Shimada N, Chiba K, Ishizaki T, Green CE, Tyson CA and Sugiyama Y (1997) Prediction of in vivo drug metabolism in the human liver from in vitro metabolism data. *Pharmacol Ther* **73**:147-171.

Jones HM, Parrott N, Jorga K and Lave T (2006) A novel strategy for physiologically based predictions of human pharmacokinetics. *Clin Pharmacokinet* **45**:511-542.

Kawai R, Lemaire M, Steimer JL, Bruelisauer A, Niederberger W and Rowland M (1994) Physiologically based pharmacokinetic study on a cyclosporin derivative, SDZ IMM 125. *J Pharmacokinet Biopharm.* **22**:327-365.

Kawai R, Mathew D, Tanaka C and Rowland M (1998) Physiologically based pharmacokinetics of cyclosporine A: extension to tissue distribution kinetics in rats and scale-up to human. *J Pharmacol Exp Ther.* **287**:457-468.

Kitazawa E, Tamura N, Iwabuchi H, Uchiyama M, Muramatsu S, Takahagi H and Tanaka M (1993) Biotransformation of pravastatin sodium (I). Mechanisms of enzymic transformation and epimerization of an allylic hydroxy group of pravastatin sodium. *Biochem Biophys Res Commun.* **192**:597-602.

Kivisto KT and Niemi M (2007) Influence of drug transporter polymorphisms on pravastatin pharmacokinetics in humans. *Pharm Res* **24**:239-247.

Komai T, Kawai K, Tokui T, Tokui Y, Kuroiwa C, Shigehara E and Tanaka M (1992) Disposition and metabolism of pravastatin sodium in rats, dogs and monkeys. *Eur J Drug Metab Pharmacokinet* **17**:103-113.

Lennernas H and Fager G (1997) Pharmacodynamics and pharmacokinetics of the HMG-CoA reductase inhibitors. Similarities and differences. *Clin Pharmacokinet* **32**:403-425.

Link E, Parish S, Armitage J, Bowman L, Heath S, Matsuda F, Gut I, Lathrop M and Collins R (2008) SLCO1B1 variants and statin-induced myopathy--a genomewide study. *N Engl J Med.* **359**:789-799.

Maeda K, Ieiri I, Yasuda K, Fujino A, Fujiwara H, Otsubo K, Hirano M, Watanabe T, Kitamura Y, Kusuhara H and Sugiyama Y (2006) Effects of organic anion transporting polypeptide 1B1 haplotype on pharmacokinetics of pravastatin, valsartan, and temocapril. *Clin Pharmacol Ther* **79**:427-439.

Miyauchi S, Sawada Y, Iga T, Hanano M and Sugiyama Y (1993) Comparison of the hepatic uptake clearances of fifteen drugs with a wide range of membrane permeabilities in isolated rat hepatocytes and perfused rat livers. *Pharm Res.* **10**:434-440.

Morimoto K, Oishi T, Ueda S, Ueda M, Hosokawa M and Chiba K (2004) A novel variant allele of OATP-C (SLCO1B1) found in a Japanese patient with pravastatin-induced myopathy. *Drug Metab Pharmacokinet.* **19**:453-455.

Nakagomi-Hagihara R, Nakai D and Tokui T (2007) Inhibition of human organic anion transporter 3 mediated pravastatin transport by gemfibrozil and the metabolites in

humans. *Xenobiotica.* **37**:416-426.

Nakai D, Nakagomi R, Furuta Y, Tokui T, Abe T, Ikeda T and Nishimura K (2001) Human liver-specific organic anion transporter, LST-1, mediates uptake of pravastatin by human hepatocytes. *J Pharmacol Exp Ther* **297**:861-867.

Naritomi Y, Terashita S, Kimura S, Suzuki A, Kagayama A and Sugiyama Y (2001) Prediction of human hepatic clearance from in vivo animal experiments and in vitro metabolic studies with liver microsomes from animals and humans. *Drug Metab Dispos* **29**:1316-1324.

Niemi M, Pasanen MK and Neuvonen PJ (2006) SLCO1B1 polymorphism and sex affect the pharmacokinetics of pravastatin but not fluvastatin. *Clin Pharmacol Ther* **80**:356-366.

Niinuma K, Kato Y, Suzuki H, Tyson CA, Weizer V, Dabbs JE, Froehlich R, Green CE and Sugiyama Y (1999) Primary active transport of organic anions on bile canalicular membrane in humans. *Am J Physiol* **276**:G1153-1164.

Nishizato Y, Ieiri I, Suzuki H, Kimura M, Kawabata K, Hirota T, Takane H, Irie S, Kusuhara H, Urasaki Y, Urae A, Higuchi S, Otsubo K and Sugiyama Y (2003) Polymorphisms of OATP-C (SLC21A6) and OAT3 (SLC22A8) genes: consequences for pravastatin pharmacokinetics. *Clin Pharmacol Ther* **73**:554-565.

Obach RS (1999) Prediction of human clearance of twenty-nine drugs from hepatic microsomal intrinsic clearance data: An examination of in vitro half-life approach and nonspecific binding to microsomes. *Drug Metab Dispos.* **27**:1350-1359.

Rane A, Wilkinson GR and Shand DG (1977) Prediction of hepatic extraction ratio from in vitro measurement of intrinsic clearance. *J Pharmacol Exp Ther.* **200**:420-424.

Roberts MS and Rowland M (1986) Correlation between in-vitro microsomal enzyme activity and whole organ hepatic elimination kinetics: analysis with a dispersion model. *J Pharm Pharmacol.* **38**:177-181.

Sawada Y, Hanano M, Sugiyama Y and Iga T (1985) Prediction of the disposition of nine

weakly acidic and six weakly basic drugs in humans from pharmacokinetic parameters in rats. *J Pharmacokinet Biopharm.* **13**:477-492.

Shitara Y, Itoh T, Sato H, Li AP and Sugiyama Y (2003) Inhibition of transporter-mediated hepatic uptake as a mechanism for drug-drug interaction between cerivastatin and cyclosporin A. *J Pharmacol Exp Ther* **304**:610-616.

Shitara Y, Horie T and Sugiyama Y (2006a) Transporters as a determinant of drug clearance and tissue distribution. *Eur J Pharm Sci* **27**:425-446.

Shitara Y and Sugiyama Y (2006b) Pharmacokinetic and pharmacodynamic alterations of 3-hydroxy-3-methylglutaryl coenzyme A (HMG-CoA) reductase inhibitors: drug-drug interactions and interindividual differences in transporter and metabolic enzyme functions. *Pharmacol Ther.* **112**:71-105.

Singhvi SM, Pan HY, Morrison RA and Willard DA (1990) Disposition of pravastatin sodium, a tissue-selective HMG-CoA reductase inhibitor, in healthy subjects. *Br J Clin Pharmacol* **29**:239-243.

Soars MG, Grime K, Sproston JL, Webborn PJ and Riley RJ (2007) Use of hepatocytes to assess the contribution of hepatic uptake to clearance in vivo. *Drug Metab Dispos.* **35**:859-865.

Takane H, Miyata M, Burioka N, Shigemasa C, Shimizu E, Otsubo K and Ieiri I (2006) Pharmacogenetic determinants of variability in lipid-lowering response to pravastatin therapy. *J Hum Genet* **51**:822-826.

Yamaoka K, Tanigawara Y, Nakagawa T and Uno T (1981) A pharmacokinetic analysis program (multi) for microcomputer. *J Pharmacobiodyn*. **4**:879-885.

Yamazaki M, Suzuki H, Hanano M, Tokui T, Komai T and Sugiyama Y (1993) Na(+)-independent multispecific anion transporter mediates active transport of pravastatin into rat liver. *Am J Physiol* **264**:G36-44.

Yamazaki M, Akiyama S, Nishigaki R and Sugiyama Y (1996a) Uptake is the rate-limiting step in the overall hepatic elimination of pravastatin at steady-state in rats. *Pharm Res*

13:1559-1564.

Yamazaki M, Kobayashi K and Sugiyama Y (1996b) Primary active transport of pravastatin across the liver canalicular membrane in normal and mutant Eisai hyperbilirubinemic rats. *Biopharm Drug Dispos* **17**:607-621.

Yamazaki M, Tokui T, Ishigami M and Sugiyama Y (1996c) Tissue-selective uptake of pravastatin in rats: contribution of a specific carrier-mediated uptake system. *Biopharm Drug Dispos* **17**:775-789.

Yamazaki M, Akiyama S, Ni'inuma K, Nishigaki R and Sugiyama Y (1997) Biliary excretion of pravastatin in rats: contribution of the excretion pathway mediated by canalicular multispecific organic anion transporter. *Drug Metab Dispos* **25**:1123-1129.

Zhang W, Chen BL, Ozdemir V, He YJ, Zhou G, Peng DD, Deng S, Xie QY, Xie W, Xu LY, Wang LC, Fan L, Wang A and Zhou HH (2007) SLCO1B1 521T-->C functional genetic polymorphism and lipid-lowering efficacy of multiple-dose pravastatin in Chinese coronary heart disease patients. *Br J Clin Pharmacol* **64**:346-352.

JPET Fast Forward. Published on November 10, 2008 as DOI: 10.1124/jpet.108.146647
This article has not been copyedited and formatted. The final version may differ from this version.

Legends for Figures

Fig. 1. Schematic diagram of the PBPK model predicting the concentration–time profiles of pravastatin. The liver compartment was divided into five compartments to mimic the dispersion model. Indicated are the blood flow (Q), the active hepatic uptake clearance (PS_{inf}), the passive diffusion clearance (PS_{dif}), the biliary clearance (PS_{bile}), and the metabolic clearance ($CL_{met,int}$), human (H) and rat (R). The enterohepatic circulation was incorporated in the case of humans.

Fig. 2. Simulated and observed plasma concentrations and biliary excretion rates for pravastatin in rats after intravenous (●, 0.2 mg/kg) or intraduodenal (○, 20 mg/kg) administration. The symbols and solid lines represent experimentally observed and simulated values, respectively. Each point represents the mean ± SE (n = 3).

Fig. 3. Simulated and observed plasma concentrations and biliary excretion rates for pravastatin in rats after the intravenous administration of various doses. The symbols and lines represent experimentally observed and simulated values, respectively. Each point represents the mean ± SE (n = 3).

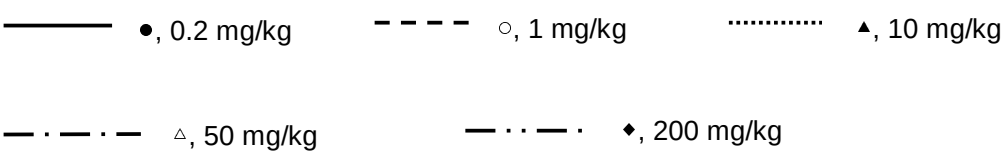

Fig. 4. Simulated and observed liver concentration profiles for pravastatin in rats after intravenous administration. Dashed and solid lines represent simulated plasma and liver concentrations, respectively. Open and closed symbols represent experimentally observed plasma and liver concentrations, respectively (circles, 10 mg/kg; triangles, 200 mg/kg). Each point represents the mean ± SE (n = 3).

Fig. 5. Simulated and observed tissue concentration profiles for pravastatin in rats after i.v. administration at 10 mg/kg. The symbols and solid lines represent experimentally observed and simulated values, respectively. Each point represents the mean ± SE (n = 3).

Fig. 6. Predicted and observed plasma concentration profiles for pravastatin in humans. Closed and open symbols represent reported plasma concentrations after intravenous (9.9 mg) and oral (19.2 mg) administration, respectively (Singhvi et al., 1990). Solid lines indicate simulated values using the parameters shown in Tables 1 and 2.

Fig. 7. Effects of changes in transporter activity on the time profiles of plasma and liver (target organ) concentrations of pravastatin in humans. Plasma and liver concentrations after oral administration (40 mg) were simulated using the PBPK model with varying hepatic transport activities over a 1/3-3-fold range of the initial values shown in Table 1. (——— ; initial, – – – ; ×1/3, ·····; ×3).

Fig. 8. Simple model to analyze the effects of changes in hepatic uptake activity and intrinsic clearance on blood and liver concentrations. Indicated are the hepatic blood flow (Q_h), renal clearance (CL_r), volume (V), concentration (C), unbound fraction (f), hepatic uptake clearance (PS_{inf}), sinusoidal efflux clearance (PS_{eff}), intrinsic clearance (CL_{int}), the blood (b), inlet (i), and liver (h).

Fig. 9. Effects of renal clearance on the impact of changes in hepatic uptake and intrinsic sequestration clearances on the AUCs of pravastatin in the blood and liver. Relative AUCs (100% as the initial value) were estimated by varying the uptake and intrinsic sequestration

clearances over a 0.1–10-fold range of the initial value when the renal clearance was 0 (———), 4 (– – –), and 16 (·····), ml/min/kg.

JPET Fast Forward. Published on November 10, 2008 as DOI: 10.1124/jpet.108.146647
This article has not been copyedited and formatted. The final version may differ from this version.

Table 1. Kinetic parameters for hepatic intrinsic clearance.

Active hepatic uptake and passive diffusion clearances on the sinusoidal membrane, biliary clearance on the canalicular membrane, and metabolic clearance were estimated by both *in vitro* and *in vivo* experiments. The details of these estimations are described in the text.

		Rat		Scaling Factor	Human	
		in vitro	*in vivo*		*in vitro*	*in vivo**
		mL/min/g liver			*mL/min/g liver*	
PS_{inf}		**2.47[a,b] (32.8)**	**9.06**	**3.7**	**0.448**	**1.66**
PS_{dif}		**0.192[a,b]**	**0.192[e]**	**1[e]**	**0.0924**	**0.0924**
PS_{bile}	**ATP-dependent**	**0.0433[c]**	**0.906[d] (92.3)**	**21**	**0.00737[c]**	**0.154**
	Nonsaturable		**0.234[d]**			**0.234[f]**
$CL_{met,int}$		**0.793 (0.846, 80.3)**	**1.33**	**1.7**	**0**	**0**

Values in parentheses indicate the K_m value (μM) for each clearance.

*Predicted by multiplying the *in vitro* parameter by the SF.

[a] (Yamazaki et al., 1993). [b] (Ishigami et al., 1995). [c] (Niinuma et al., 1999).

[d] (Yamazaki et al., 1997). [e] Assumed that the SF for PS_{dif} is one.

[f] Assumed negligible interspecies difference between rat and human.

Table 2. Physiological and kinetic parameters for modeling in rats and humans

	Rat	Human
Physiological parameters		
Weight (g/kg) [a]		
Liver	41.2	24.1
Extracellular space in liver	11.5	6.7
Brain	6.8	5.3
Lung	4.0	16.7
Muscle	488	429
Kidney	9.2	4.43
Blood flow rate[a] (mL/min/kg)		
Liver	55.2	20.7
Brain	5.3	10.0
Lung	172	74.9
Muscle	30.0	10.7
Kidney	36.9	15.7
Kinetic parameters		
Plasma unbound fraction[b]	0.64	0.47
Liver unbound fraction	0.51[c]	0.51[d]
Blood-to-plasma ratio[e]	0.59	0.56
Fraction absorbed	0.62[f]	0.47[g]
Renal clearance (mL/min/kg)	1.5[h]	11.3[i]
Absorption rate constant (min^{-1})[j]	0.0088	0.0078
Tissue-to-blood concentration ratio		
Brain	0.036	0.033[k]
Lung	0.74	0.67[k]
Muscle	0.22	0.20[k]
Kidney	14	13[k]

[a] The volume and blood flow rate in each tissue were taken from (Davies and Morris, 1993), and (Kawai et al., 1994). The tissue volume was converted to tissue weight based on the assumption that the tissue gravity is 1 g/mL.

[b] (Yamazaki et al., 1996c) and manufacturer's interview form. [c] (Yamazaki et al., 1996b).

[d] Assumed negligible interspecies difference between rat and human.

[e] (Yamazaki et al., 1996c) and (Lennernas and Fager, 1997). [f] (Komai et al., 1992).

[g] Estimated from the bioavailability (0.18) and hepatic availability (0.38) (Singhvi et al., 1990).

[h] Obtained from the urinary excretion data for i.v. administration of 10 mg/kg.

[i] (Singhvi et al., 1990). [j] Estimated by noncompartment analysis.

[k] Estimated by $K_p = f_B/f_T$.

JPET Fast Forward. Published on November 10, 2008 as DOI: 10.1124/jpet.108.146647
This article has not been copyedited and formatted. The final version may differ from this version.

Table 3. Changes in the AUCs (% of the control) for plasma and liver concentrations of pravastatin after its oral administration when the transporter function changes.

Change in clearance	PS_{inf}		PS_{bile}		PS_{dif}	
	plasma	liver	plasma	liver	plasma	liver
×1	100	100	100	100	100	100
×1/3	271	68	143	255	83	103
×3	14	115	84	38	146	92

Fig. 1

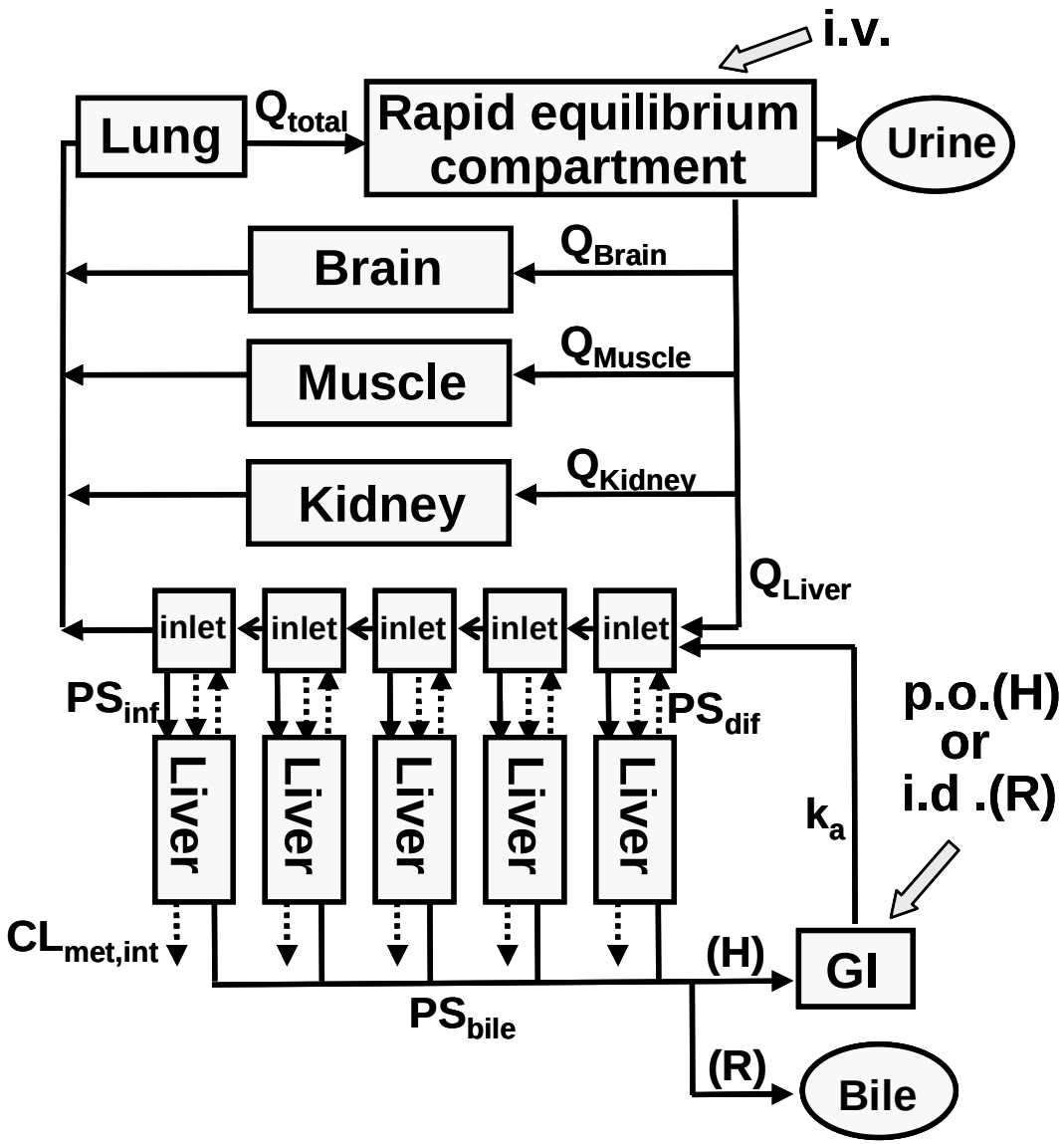

Fig. 2

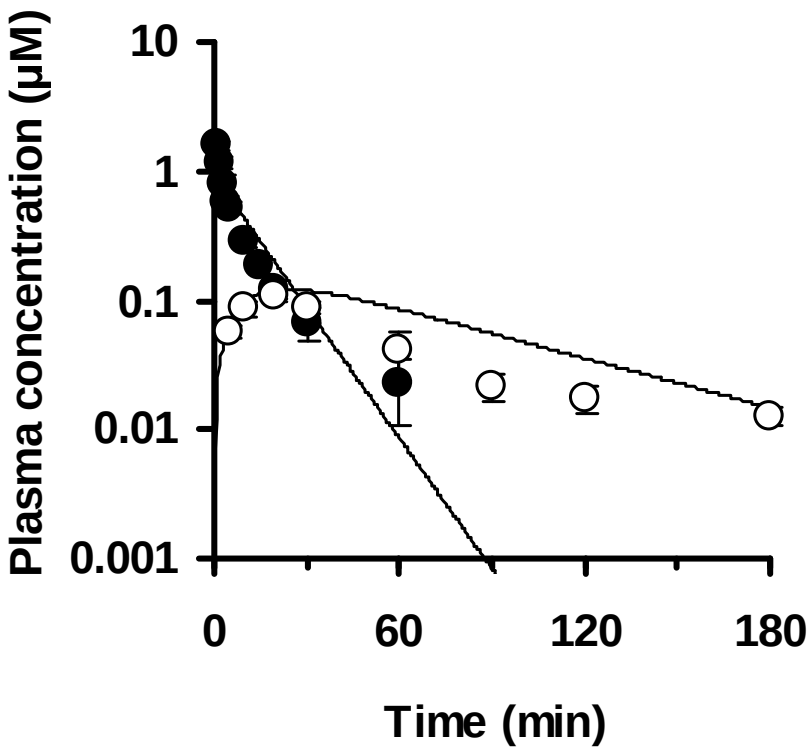

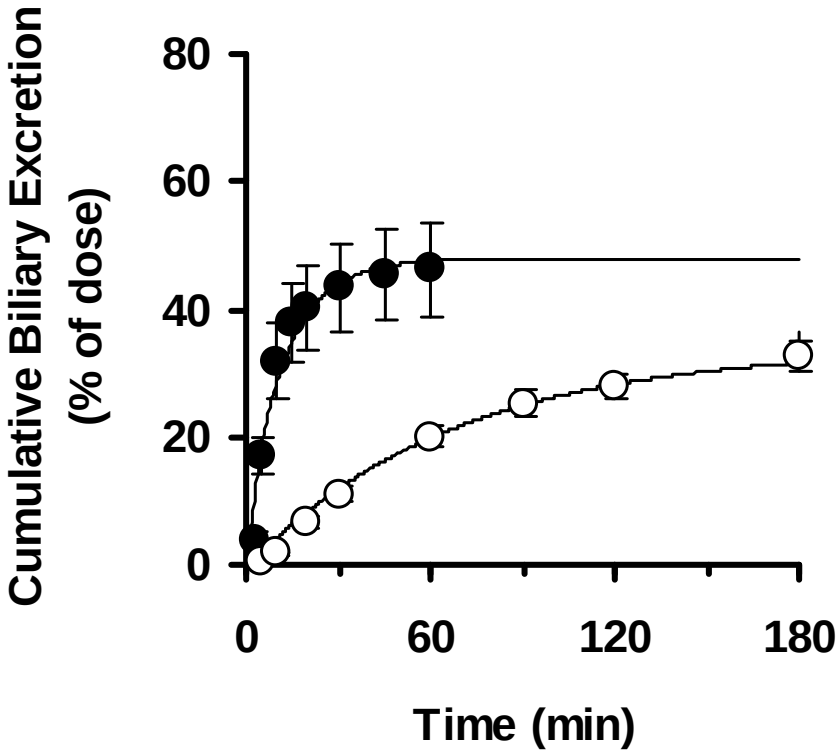

Fig. 3

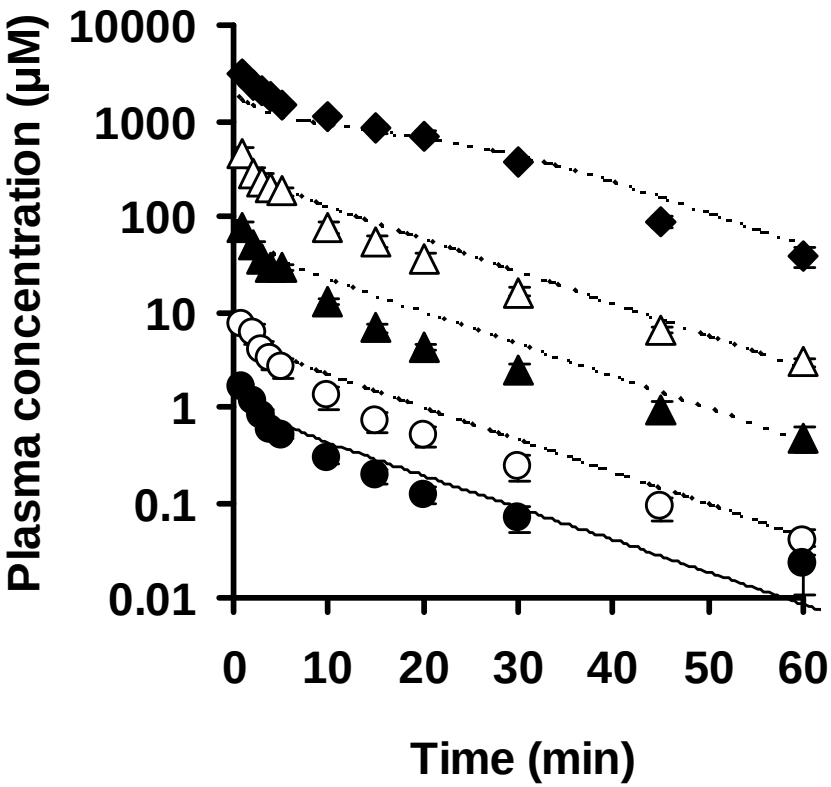

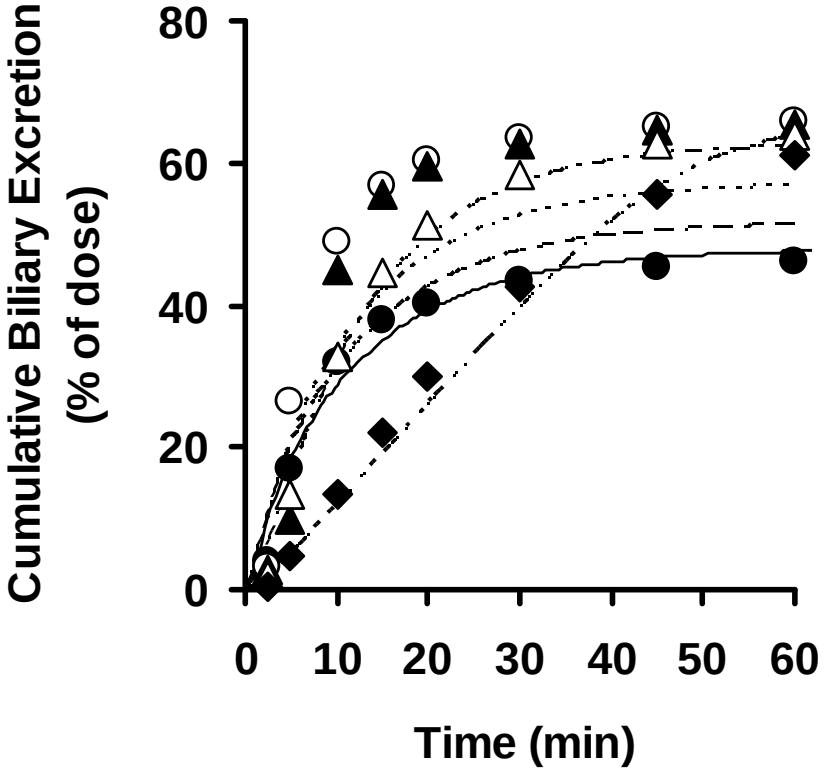

Fig. 4

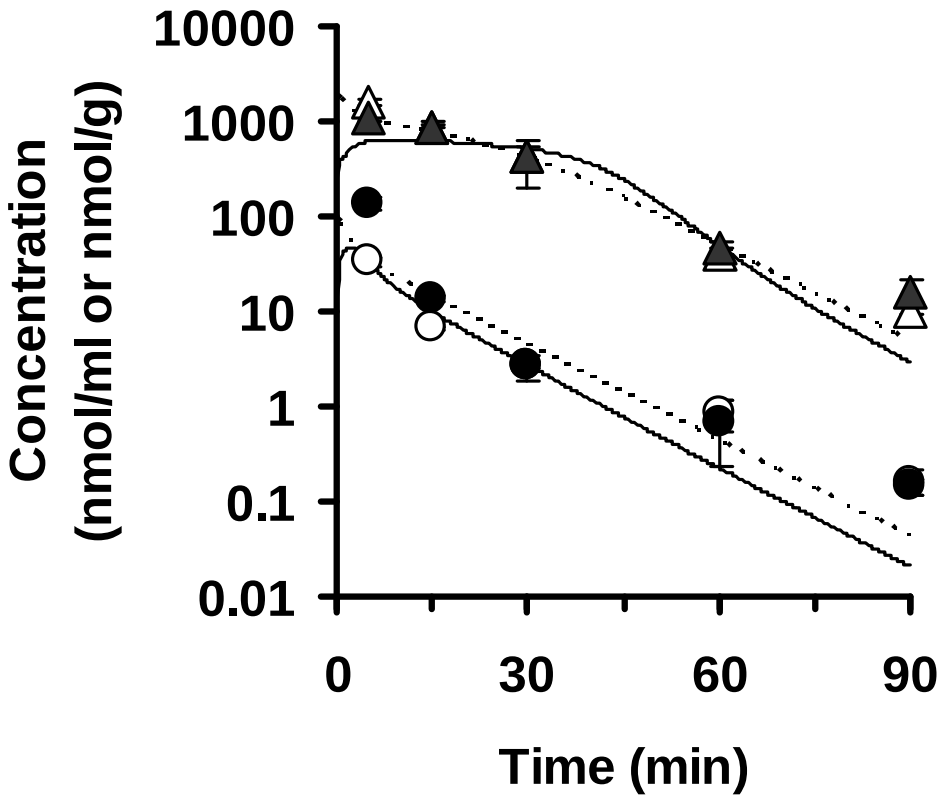

Fig. 5

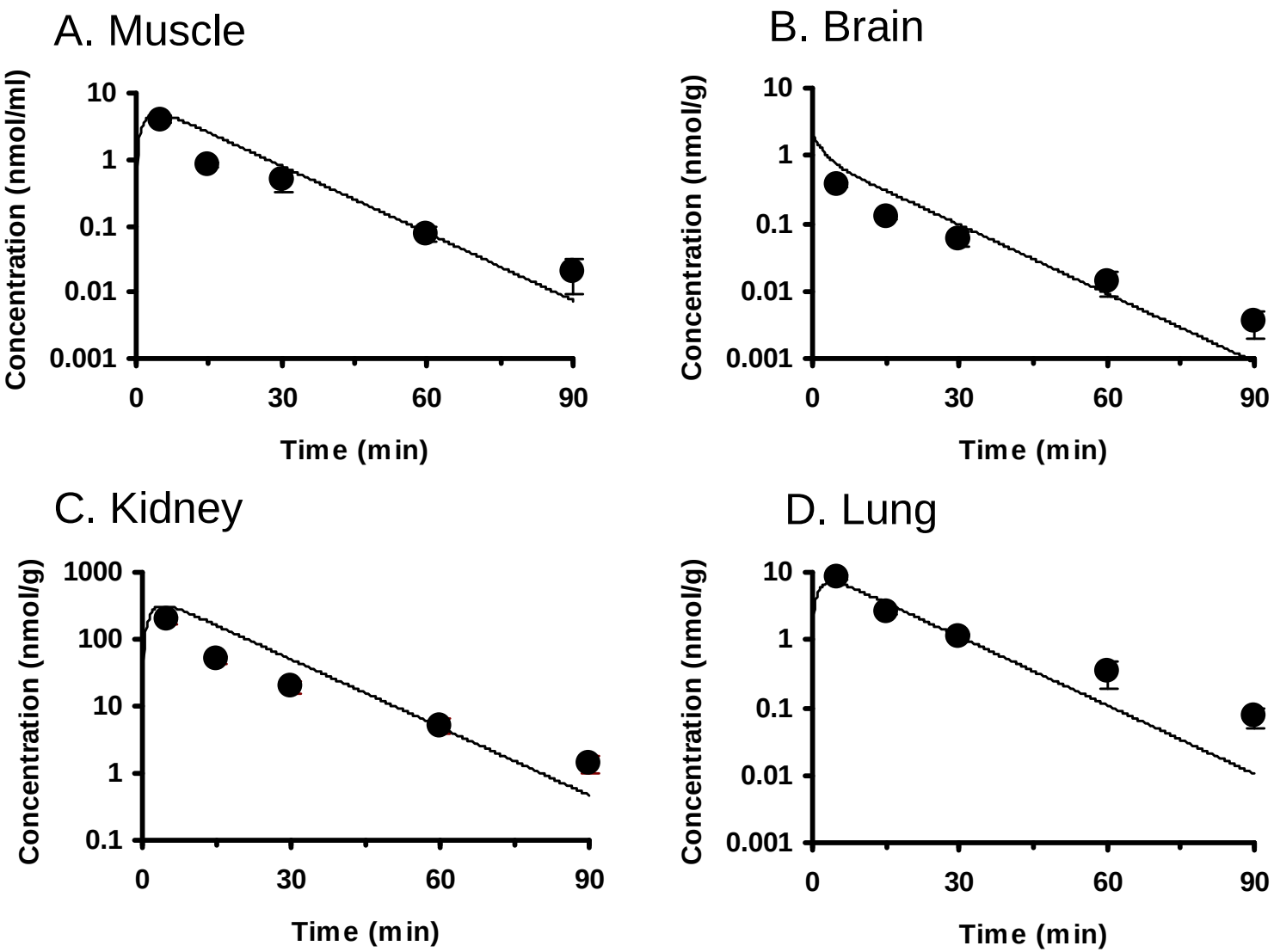

Fig. 6

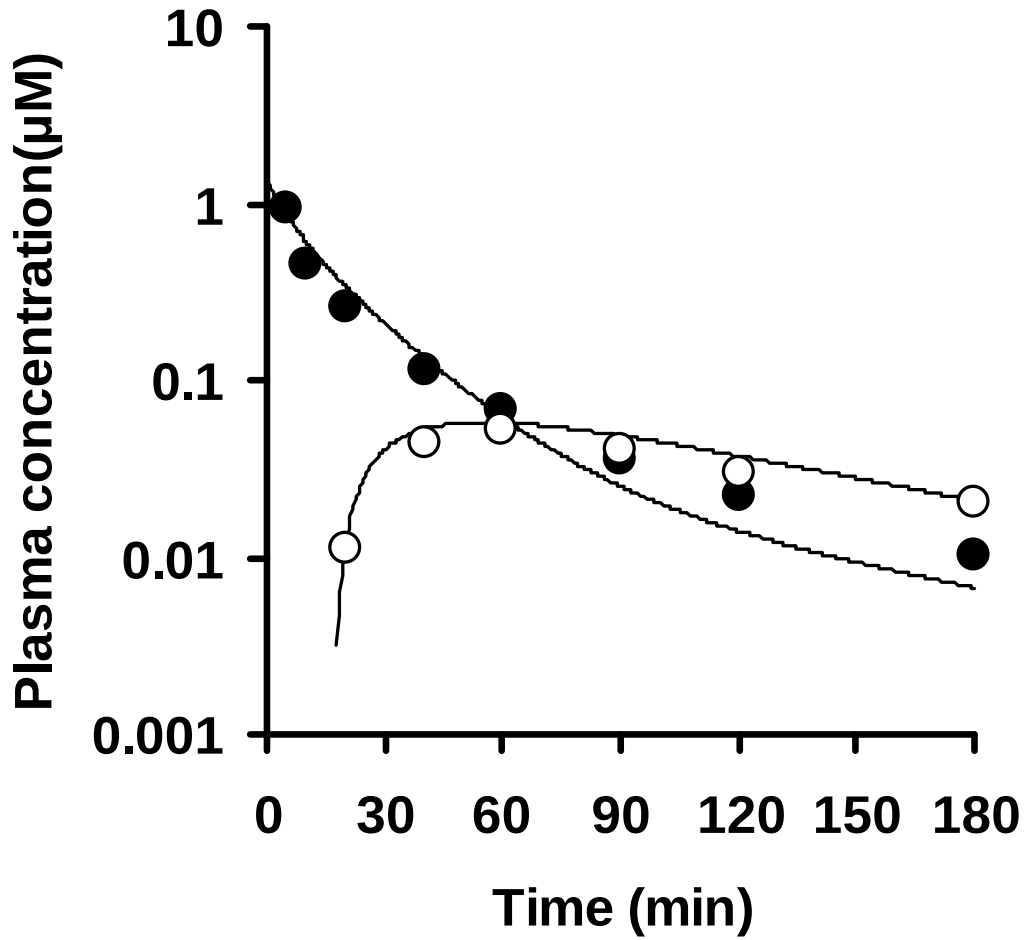

Fig. 7

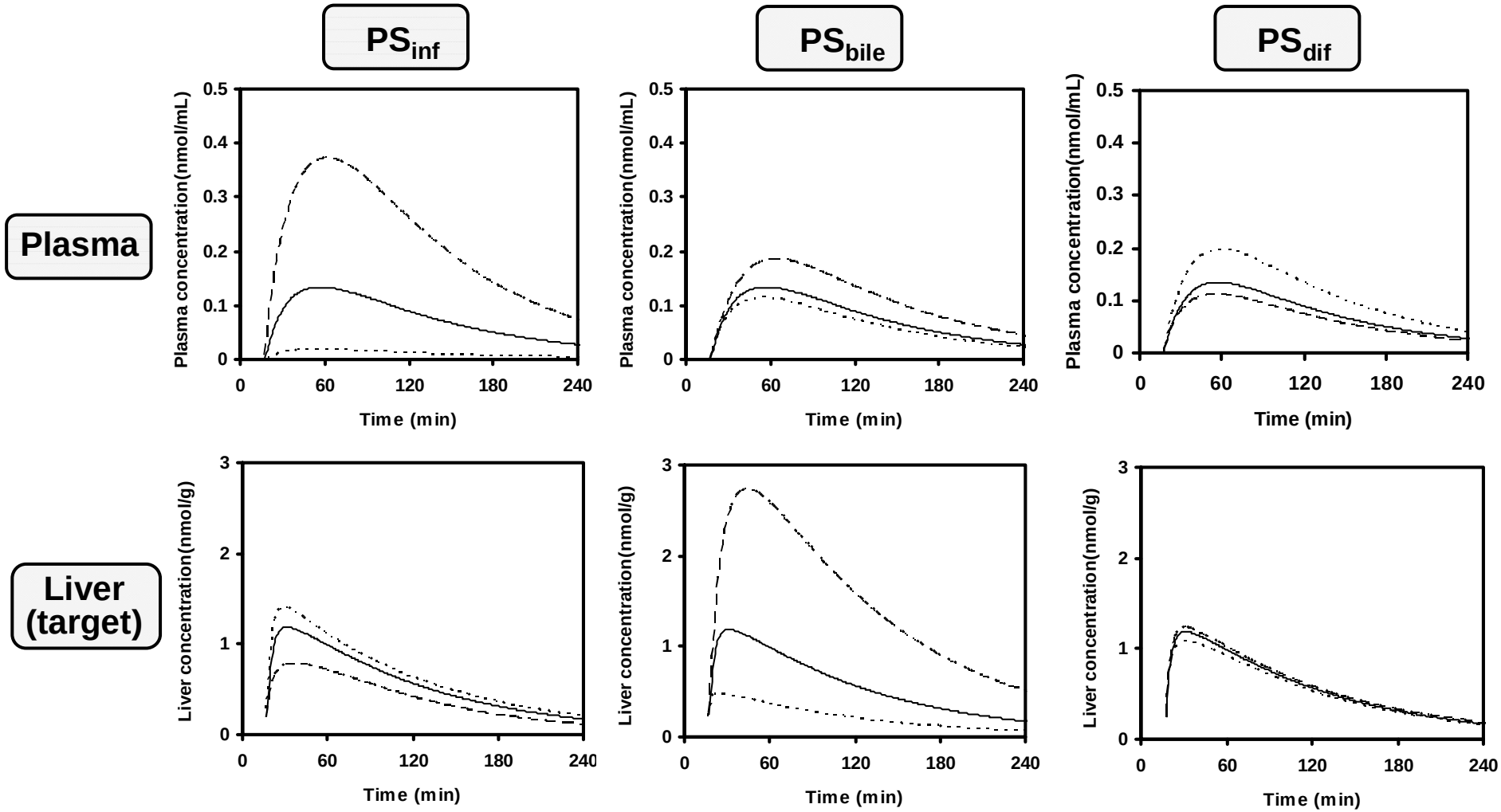

Fig. 8

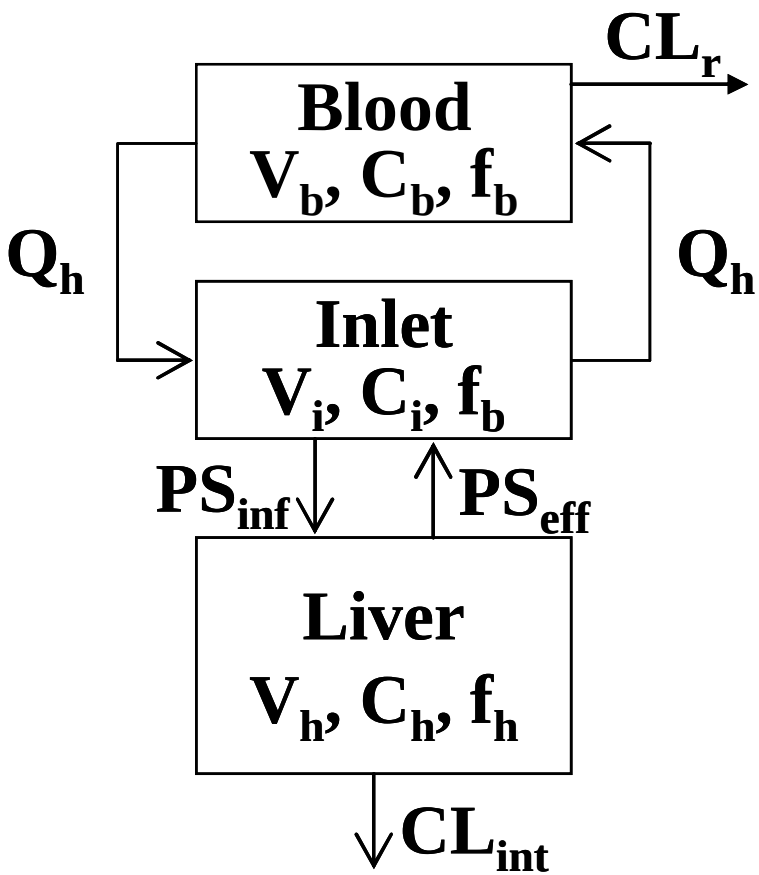

Fig. 9

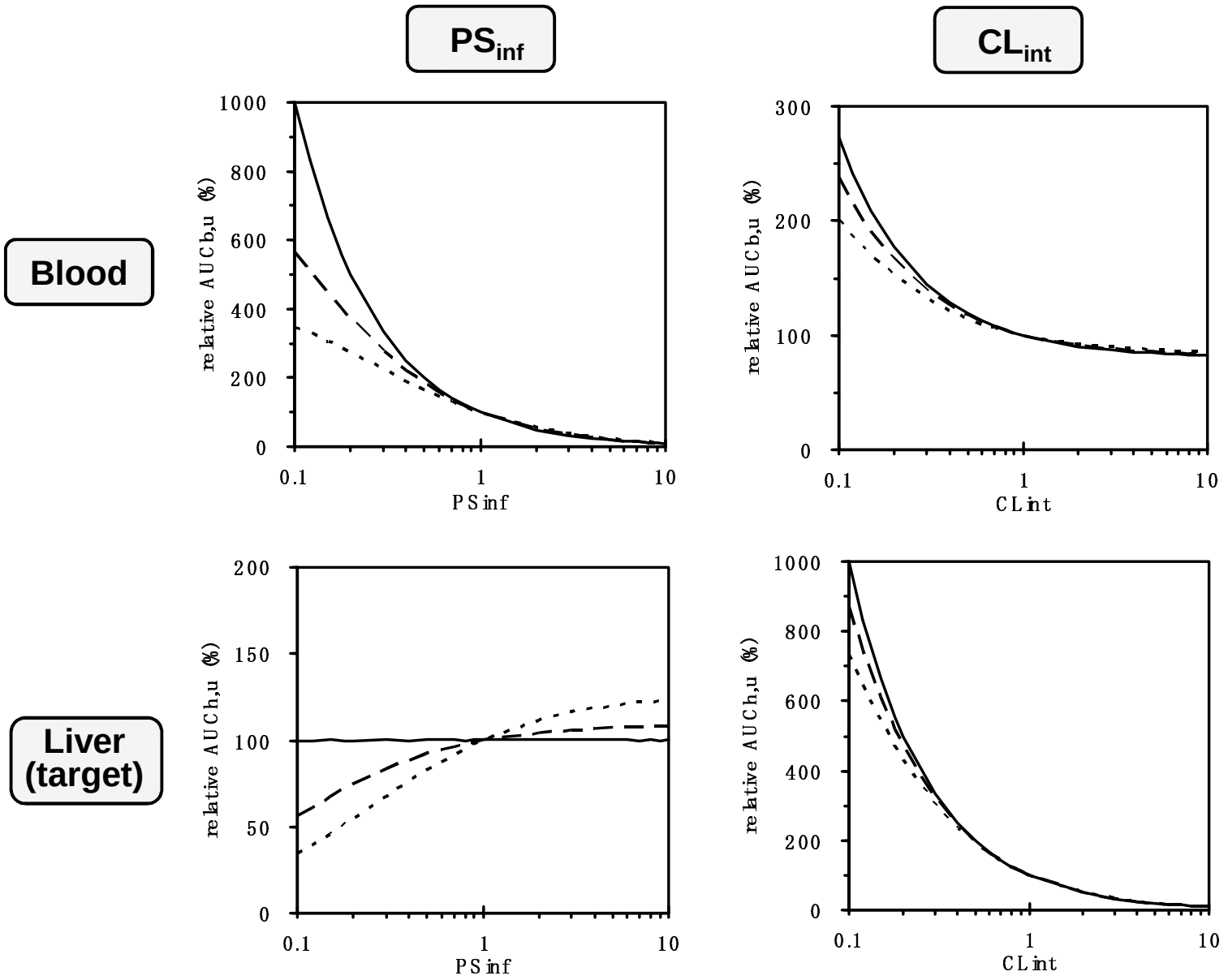

JPET Fast Forward. Published on November 10, 2008 as DOI: 10.1124/jpet.108.146647
This article has not been copyedited and formatted. The final version may differ from this version.

Appendix I: Differential Mass Balance Equations for the PBPK Model

(1) Nomenclature

General

Q, blood flow rate; V, tissue weight; C, pravastatin concentration; K_p, tissue-to-blood partition coefficient; f_B, blood unbound fraction; f_T, tissue unbound fraction; V_m, maximum transport velocity; K_m, half-saturation concentration for transport; CL_R, renal clearance; PS_{inf}, intrinsic hepatic uptake clearance; PS_{dif}, passive diffusion clearance on the sinusoidal membrane; PS_{bile}, intrinsic biliary clearance; CL_{met}, intrinsic metabolic clearance; Fa, fraction absorbed

Subscripts

B, blood; LU, lung; BR, brain; MU, muscle; R, kidney; GI, gastrointestinal tract; H, liver; HE, liver extracellular space; inf, influx; met, metabolism

(2) Model Equations

Hepatic uptake, biliary excretion, and metabolic clearances in humans were linear parameters.

Blood pool:

$$V_B(dC_B/dt) = Q_{LU}(C_{LU}/K_{p,LU} - C_B) - CL_RC_B$$

Lung:

$$V_{LU}(dC_{LU}/dt) = Q_{BR}C_{BR}/K_{p,BR} + Q_{MU}C_{MU}/K_{p,MU} + Q_RC_R/K_{p,R} + Q_HC_{HE5} - Q_{LU}C_{LU}/K_{p,LU}$$

Brain, Muscle, Kidney:

$$V_i(dC_i/dt) = Q_i(C_B - C_i/K_{p,i})$$

JPET Fast Forward. Published on November 10, 2008 as DOI: 10.1124/jpet.108.146647
This article has not been copyedited and formatted. The final version may differ from this version.

Liver 1–5:

(1) rat $(V_{Hi}/5)(dC_{Hi}/dt) = (V_{m,inf}/5)f_BC_{HEi}/(K_{m,inf} + f_BC_{HEi}) + (PS_{dif}/5)f_BC_{HEi}$

$$- (PS_{dif}/5)f_TC_{Hi} - (V_{m,bile}/5)f_TC_{Hi}/(K_{m,bile} + f_TC_{Hi})$$

$$- (V_{m,met}/5)f_TC_{Hi}/(K_{m,met} + f_TC_{Hi})$$

(2) human $(V_{Hi}/5)(dC_{Hi}/dt) = (PS_{inf}/5)f_BC_{HEi} + (PS_{dif}/5)f_BC_{HEi} - (PS_{dif}/5)f_TC_{Hi}$

$$- (PS_{bile}/5)f_TC_{Hi} - (CL_{met}/5)f_TC_{Hi}$$

Liver extracellular compartment 1:

(1) rat $(V_{HE1}/5)(dC_{HE1}/dt) = Q_H(C_B - C_{HEi}) - (V_{m,inf}/5)f_BC_{HEi}/(K_{m,inf} + f_BC_{HEi})$

$$- (PS_{dif}/5)f_BC_{HEi} + (PS_{dif}/5)f_TC_{Hi}$$

(2) human $(V_{HE1}/5)(dC_{HE1}/dt) = Q_H(C_B - C_{HEi}) - (PS_{inf}/5)f_BC_{HEi} - (PS_{dif}/5)f_BC_{HEi}$

$$+ (PS_{dif}/5)f_TC_{Hi} + k_aF_aX_{GI}$$

Liver extracellular compartments 2–5:

(1) rat $(V_{HEi}/5)(dC_{HEi}/dt) = Q_H(C_{HE(i-1)} - C_{HEi}) - (V_{m,inf}/5)f_BC_{HEi}/(K_{m,inf} + f_BC_{HEi})$

$$- (PS_{dif}/5)f_BC_{HEi} + (PS_{dif}/5)f_TC_{Hi}$$

(2) human $(V_{HEi}/5)(dC_{HEi}/dt) = Q_H(C_{HE(i-1)} - C_{HEi}) - (PS_{inf}/5)f_BC_{HEi} - (PS_{dif}/5)f_BC_{HEi}$

$$+ (PS_{dif}/5)f_TC_{Hi}$$

Bile or GI tract:

(1) rat $X_{bile} = \sum((V_{m,bile}/5)f_TC_{Hi}/(K_{m,bile} + f_TC_{Hi}))$

(2) human $X_{GI} = \sum(PS_{bile}/5)f_TC_{Hi} - (k_a/Fa)X_{GI}$

JPET Fast Forward. Published on November 10, 2008 as DOI: 10.1124/jpet.108.146647
This article has not been copyedited and formatted. The final version may differ from this version.

Appendix II: Effect of Renal Clearance on the Impact of the Change in the Uptake Clearance on the AUCs of the Plasma and Liver

Q_h and CL_r represent the hepatic blood flow and renal clearance, respectively. PS_{inf}, PS_{eff}, and CL_{int} are hepatic uptake, sinusoidal efflux, and intrinsic sequestration clearances, respectively. V and C represent volume and concentration, respectively. Subscripts b, i, and h represent blood, inlet, and liver, respectively. Mass balance differential equations for each compartment in the simple model shown in Fig. 8 are as follows:

$$V_b \cdot \frac{dC_b}{dt} = Q_h(C_i - C_b) - CL_r \cdot C_b$$
$$V_i \cdot \frac{dC_i}{dt} = Q_h(C_b - C_i) - f_b \cdot PS_{inf} \cdot C_i + f_h \cdot PS_{eff} \cdot C_h$$
$$V_h \cdot \frac{dC_h}{dt} = f_b \cdot PS_{inf} \cdot C_i - f_h \cdot (PS_{eff} + CL_{int}) \cdot C_h$$

Integrating these equations gives:

$$\frac{Dose}{f_b \cdot AUC_b} = \frac{PS_{inf} \cdot CL_{int}}{PS_{eff} + CL_{int}} \cdot \frac{CL_r + Q_h}{Q_h} + \frac{CL_r}{f_b} \quad \text{(A1)}$$
$$\frac{Dose}{f_h \cdot AUC_h} = CL_{int} + \frac{Q_h \cdot CL_r}{CL_r + Q_h} \cdot \frac{PS_{eff} + CL_{int}}{f_b \cdot PS_{inf}} \quad \text{(A2)}$$

where AUC_b and AUC_h represent the area under the concentration–time curve for the blood and liver, respectively. Substituting $CL_R = 0$ yields:

$$\frac{Dose}{f_b \cdot AUC_b} = PS_{inf} \cdot \frac{CL_{int}}{PS_{eff} + CL_{int}} \quad \text{(A3)}$$
$$\frac{Dose}{f_h \cdot AUC_h} = CL_{int} \quad \text{(A4)}$$

Accordingly, AUC_h depends only on CL_{int} when the renal clearance is negligible. In contrast,

JPET Fast Forward. Published on November 10, 2008 as DOI: 10.1124/jpet.108.146647
This article has not been copyedited and formatted. The final version may differ from this version.

AUC_b is inversely proportional to PS_{inf}. If the renal clearance is maximal, that is, the renal blood flow (Q_r), Eq. (A2) can be converted to:

$$\frac{Dose}{f_h \cdot AUC_h} = CL_{int} + Q \cdot \frac{PS_{eff} + CL_{int}}{f_b \cdot PS_{inf}} \qquad \text{(A5)}$$

$$where \quad Q = \frac{Q_h \cdot Q_r}{Q_r + Q_h} \approx 9$$

When the hepatic uptake is the rate-limiting process, so $CL_{int} >> PS_{eff}$, Eq. (A5) can be converted to:

$$R = \frac{Dose}{f_h \cdot AUC_h} = CL_{int}\left(1 + Q \cdot \frac{CL_{int}}{f_b \cdot PS_{inf}}\right) \qquad \text{(A6)}$$

Accordingly, the R value can be higher than CL_{int} by up to $Q \times CL_{int} / (f_b \times PS_{inf})$.

Figure 9 shows the effects of renal clearance on the impact of the changes in hepatic uptake and intrinsic sequestration clearance on the AUCs of pravastatin in the plasma and liver. A simulation was performed using Eqs (A1) and (A2) and the parameters shown in Tables 1 and 2, when the renal clearance was 0, 4 (quarter of the renal blood flow), and 16 (the renal blood flow) mL/min per kg body weight.